Journal of Civil Engineering and Construction 2025;14(3):107-125
https://doi.org/10.32732/jcec.2025.14.3.107

Innovative Shear Link with A Corrugated and Perforated Web for Steel Moment-Resisting Frames

Mahmoud Ali[1], Fereshteh Emami[2], Ali Khalaf[2]

1. School of Civil Engineering, College of Engineering, University of Tehran, Tehran, Iran
2. Department of Civil Engineering, Science and Research Branch, Islamic Azad University, Tehran, Iran
E-mail: mahmoud.ali@ut.ac.ir; f-emami@srbiau.ac.ir

Received: 13 March 2025; Accepted: 23 May 2025; Available online: 15 June 2025

Abstract: Seismic codes specify minimum span-to-depth ratios for beams in moment-resisting frames (MRFs) to ensure adequate length for the development of flexural hinges at the beam ends, set at 7 and 5 for special and intermediate moment frames, respectively. To challenge this limitation, this paper introduces an innovative approach using replaceable shear links positioned at the mid-span of flexural beams, allowing for deviations from the prescribed ratios. Specifically, a shear link with a corrugated and perforated web was proposed, offering advanced performance in MRFs. A numerical study using the finite element method was performed to investigate the cyclic performance of moment-resisting frames equipped with the proposed shear link, incorporating key parameters such as corrugation angle, hole shape, and holes layout. The results were benchmarked against both a conventional moment-resisting frame and a frame featuring a flat perforated web with stiffeners for comparison. The proposed shear links exhibited superior energy dissipation, stable performance, acceptable lateral capacity, and high ductility. For all models, plastic strains were concentrated in the fuse region, while the other components remained elastic. The corrugation angle of 30° proved optimal, offering the highest lateral capacity compared to angles of 45° and 60° evaluated for the web plate. The diameter-to-spacing (D/S) ratio had a minimal effect on lateral capacity when the corrugation angle was fixed at 30°. Additionally, optimizing the hole layout with smaller, more uniformly distributed perforations allowed the proposed models to match the lateral capacity of conventional moment frames, making them a viable alternative to traditional designs.
Keywords: Shear link; Perforated; Corrugated; Moment-resisting frames; Numerical analysis.

1. Introduction

Steel moment-resisting frames (MRFs) are widely employed as lateral load-resisting systems, primarily for their high ductility and adaptability in architectural design. However, achieving the desired stiffness in these frames often necessitates larger members [1], due to the high ductility required by flexural plastic hinge formations at beam and column bases [2]. On the other hand, seismic codes such as AISC-341 [3] specify a minimum span-to-depth ratio to ensure the formation of sufficient flexural plastic hinges at beam ends and to mitigate the risk of shear failure (set at 5 and 7 for intermediate and special moment frames, respectively), which can become more pronounced as this ratio decreases. This requirement can conflict with stiffness needs, particularly in tubular structures where only exterior frames provide lateral resistance, while interior frames primarily support gravity loads. In such systems, maintaining a span-to-depth ratio between 3.5 and 4 is essential to achieve the expected cantilever-type behavior and adequately control structural drift [4].

To address the aforementioned limitations associated with moment-resisting frames (MRFs), a novel approach has recently been proposed: the incorporation of a replaceable shear link at the beam's mid-span, designed to function as a shear fuse. During seismic events, energy is dissipated through shear yielding of this fuse, which has a lower shear capacity than the primary beam. This mechanism transfers plastic hinging from the beam ends to the mid-span, as the link yields before the main beam. Consequently, this approach removes the need for minimum span-to-depth ratios to ensure adequate plastic hinge length at the beam ends, as specified in seismic codes for MRFs. Furthermore, positioning the link at mid-span, near the inflection point where bending moments approach zero, effectively decouples strength and stiffness, where weakening the beam's mid-length in this way minimally impacts flexural stiffness while significantly enhancing ductility [1, 5].

For the proposed system, several approaches have been explored to weaken the beam's mid-span link region. These include using a shear link with a reduced cross-section relative to the main beam [6], a slitted web section composed of small beams or strips [7], a perforated and stiffened web to prevent local buckling [5, 8], a rectangular opening with rounded corners in its web [9], and a reduced cross-section with a corrugated web [10]. However,

reducing the cross-section of the link beam can substantially impact its shear capacity. Additionally, adding stiffeners within a perforated web may increase costs and induce residual stresses from welding, heightening the risk of web fracture due to low-cycle fatigue [11].

To address these challenges, this study proposes a novel shear link for moment-resisting frames that features a perforated corrugated web plate, as depicted in Fig. 1. The proposed approach weakens the shear link without reducing the mid-beam cross-section, thus minimizing any significant impact on the beam's shear capacity while enhancing ductility. Additionally, the corrugated web plate provides high out-of-plane buckling resistance [12], eliminating the need for stiffeners within the link. This strategy retains the conventional configuration of typical shear links while significantly minimizing residual stresses associated with welding and reducing the overall steel consumption due to the elimination of internal stiffeners. The simplification in fabrication and the decreased welding requirements directly contribute to a more economical and efficient solution, without compromising structural performance. Furthermore, the link is designed to be fully replaceable, promoting ease of construction as well as straightforward post-earthquake repair and maintenance. Its bolted connection to adjacent beam segments enables rapid installation and replacement, enhancing its practicality for real-world engineering applications.

Given the effective performance of corrugated steel plates, they have been applied in various structural components, including bridge plate girders [13, 14], steel plate shear walls [15-22], and coupling steel beams [23, 24]. As shown in Fig. 1, the trapezoidal corrugation shape was considered for the shear link across all models, as it demonstrated superior performance compared to other corrugation shapes [25]. The frame was analyzed numerically under cyclic loading conditions, investigating the effects of varying corrugation angles, hole shapes, and arrangements of holes with different diameters on the overall performance of the improved moment frame system with short spans. The results were compared to reference specimens of a conventional moment-resisting frame and a moment frame featuring a flat web plate with perforations and stiffeners, all sharing the same characteristics. The following subsection presents the design formulas related to the proposed shear link.

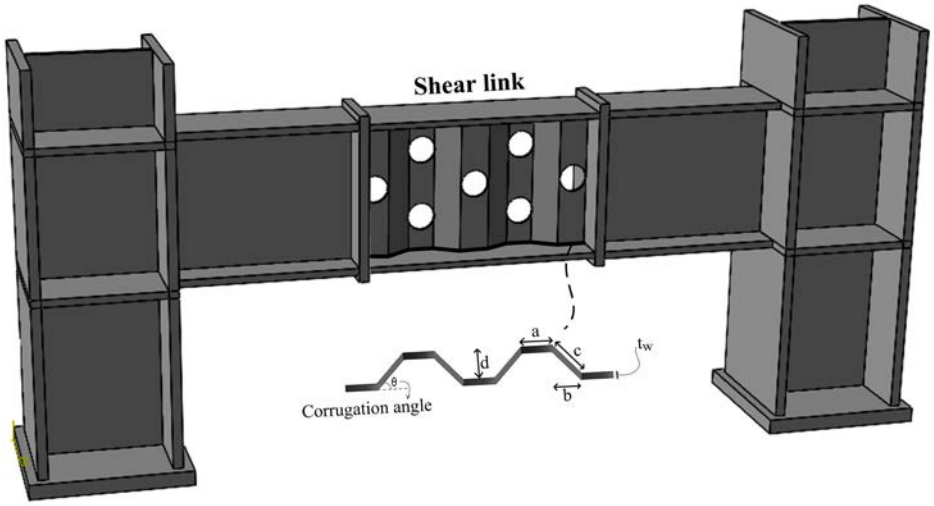

Fig. 1. Illustrations of the proposed shear link integrated into a moment-resisting frame

2. Approach and design criteria

The design of the proposed link should ensure that its shear strength (V_n) remains lower than the shear force associated with the development of flexural plastic hinges at the beam ends (V_p) [3]. This condition can be achieved as follows:

$$V_n \leq \emptyset V_p \tag{1}$$

$$V_p = \frac{2M_{pb}}{L} \tag{2}$$

where $\emptyset$ is the resistance factor for shear equals 0.9 according to AISC-360 [26], M_{pb} is the plastic bending moment of the beam ($M_{pb} = Z_b F_y$), Z_b is the plastic section modulus of the beam cross-section, F_y is the yielding strength of the beam, and L is the clear span of the beam.

The shear strength of a shear link with a flat web plate can be calculated according to the AISC-360 [26] as Eq. 3, where F_{yl} is the yielding strength of the link's web, A_w is the cross-sectional web area, h_w is the depth of the web, and t_w is the thickness of the web.

$$V_n = 0.6F_{yl}A_w = 0.6F_y h_w t_w \tag{3}$$

To account for the presence of web perforations, the shear strength of the perforated shear link can be calculated using the shear strength reduction factor $(1 - D/S)$ proposed by Bruneau et al. [27], originally developed for perforated steel plate shear walls, as follows:

$$V_n = (1 - D/S)\ 0.6F_{yl}A_w \tag{4}$$

where D is the hole's diameter and S is the spacing between centers of adjacent holes. However, when a trapezoidal corrugated web plate is used within the link, the shear strength should be calculated based on the specific shear strength of the corrugated web plate (τ_n) [10], as determined by the following equation:

$$V_n = \tau_n A_w \tag{5}$$

According to PC bridges with corrugated steel webs [28], the shear strength τ_n can be calculated according to the shear yielding strength τ_y as:

$$\frac{\tau_n}{\tau_y} = \begin{cases} 1 \\ 1 - 0.614(\lambda_s - 0.6) \\ 1/{\lambda_s}^2 \end{cases} \quad \begin{cases} for\ \lambda_s < 0.6 \\ for\ 0.6 \le \lambda_s \le \sqrt{2} \\ for\ \lambda_s > \sqrt{2} \end{cases} \tag{6}$$

where $\tau_y = 0.6F_{yl}$. According to the above equations, the web will undergo shear yielding if the condition $\lambda_s < 0.6$. is met. Thus, to ensure the shear yielding of the corrugation web plate, the proposed shear link design should satisfy this criterion. The parameter λ_s can be calculated using the following equation:

$$\lambda_s = \sqrt{\tau_y / \tau_{cr}^e} \tag{7}$$

where τ_{cr}^e is the elastic buckling shear strength that can be obtained as:

$$\left(\frac{1}{\tau_{cr}^e}\right)^n = \left(\frac{1}{\tau_{cr.L}}\right)^n + \left(\frac{1}{\tau_{cr.G}}\right)^n \tag{8}$$

$$\tau_{cr.L} = K_L \frac{\pi^2 E}{12(1 - \nu^2)} \left(\frac{t_w}{w}\right)^2 \tag{9}$$

$$\tau_{cr.G} = K_G \frac{(D_y {D_x}^3)^{1/4}}{{h_w}^2 t_w} \tag{10}$$

where $\tau_{cr.L}$ is the elastic local shear buckling strength, $\tau_{cr.G}$ is the elastic global shear buckling strength, *n* equals 2 for trapezoidal corrugation plates, K_L is the local shear buckling coefficient, E is the elastic modulus, ν is Poisson's ratio of steel, w is the maximum value between "a" and "c" shown in Fig. 1, t_w is the thickness of web plate shown in Fig. 1, K_G is global shear buckling coefficient equals to 36 for simple supports condition of the web [29], and D_x and D_y are the flexural stiffness of the corrugated plates around the "x" and "y" axes, respectively. These parameters can be calculated as follows:

$$K_L = 5.34 + 4.0\left(\frac{w}{h_w}\right)^2 \tag{11}$$

$$D_x = \frac{E{t_w}^3[(d/t_w)^2 + 1]}{6\eta} \tag{12}$$

$$D_y = \frac{E{t_w}^3}{12(1-\nu^2)}\eta \tag{13}$$

$$\eta = \frac{(a+b)}{(a+c)} \tag{14}$$

3. Numerical simulation

This subsection presents a detailed numerical analysis of moment-resisting frames incorporating shear links located at the beam midspan. The study began with a validation process, using experimental data from a moment-resisting frame equipped with a shear link that featured a flat, perforated web plate with stiffeners [5]. A parametric study was subsequently conducted to investigate alternative design configurations, focusing on moment-resisting frames with shear links featuring corrugated and perforated web plates under cyclic loading. Key parameters, such as the corrugation angle, holes shape, and holes layout, were analyzed, with models for each parameter grouped separately to provide a clear and comprehensive illustration. Comparative analyses were then performed between these groups. The numerical results for each model were compared to reference specimens, including a conventional moment-resisting frame [6] and a frame with a shear link utilizing a flat, perforated web plate with stiffeners [5].

3.1 Verification study

The numerical analysis was carried out using the finite element method (FEM) via Abaqus software [30]. The experimental specimen "Pw-MRF," conducted by Mirghaderi et al. [5], was used as a benchmark to validate the simulation methodology employed in this study. Fig. 2 provides a detailed illustration of the specimen's geometrical and sectional properties, which consist of a one-bay moment-resisting frame featuring a shear link with a flat, perforated web plate reinforced by stiffeners.

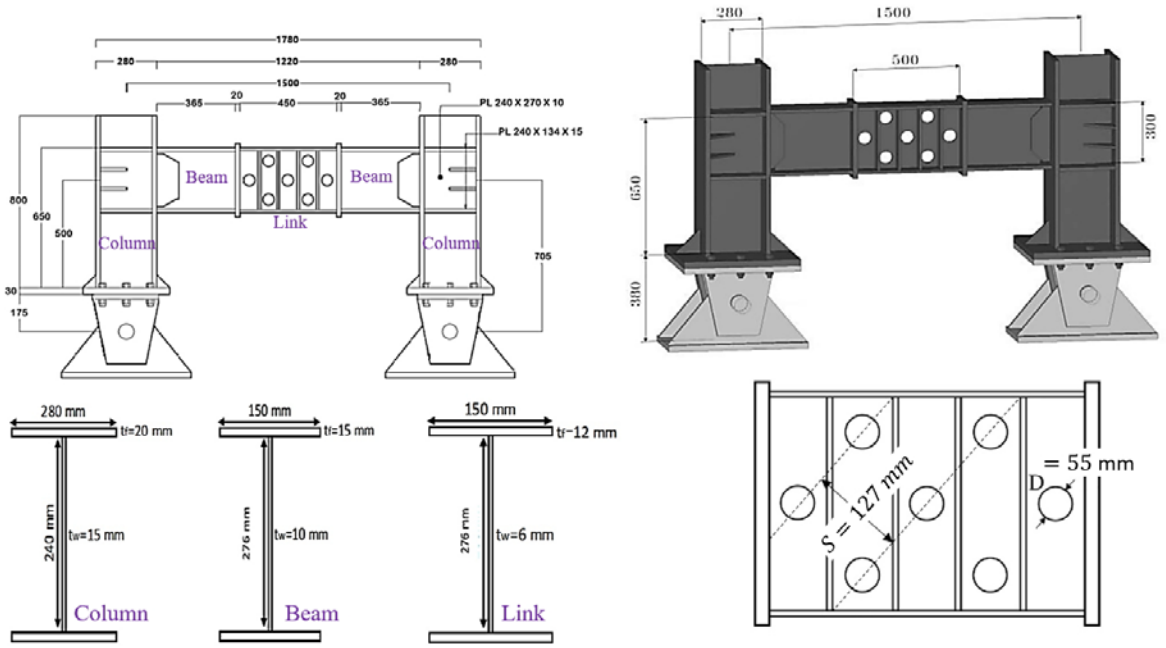

Fig. 2. Geometrical and sectional properties of the modeled specimen [5]

Fig. 3 illustrates the constraints applied in the model. Based on experimental observations, no separation was detected at the column-to-beam or beam-to-link welds, so the "Tie surfaces" constraint was applied between these steel parts [31-36]. Additionally, no tearing was observed in the welds between the stiffeners and web plate, the column and base plate, or the column and continuity plates. Therefore, to simplify the model, the link beam and stiffeners, as well as the column and its connected components, were each merged into single parts.

As shown in Fig. 3, instead of directly modeling pinned supports for each column, reference points (RP-1 and RP-2) were defined at the pin locations, with each point linked to the bottom surface of the corresponding column's base plate using a "Rigid body" constraint. Additionally, to prevent stress concentration at the load application point, a reference point, "RP-3," was defined at the hydraulic jack location and coupled to the surface where the

load was applied (the portion of the left column's flange where the hydraulic jack was attached) using a "Coupling" constraint.

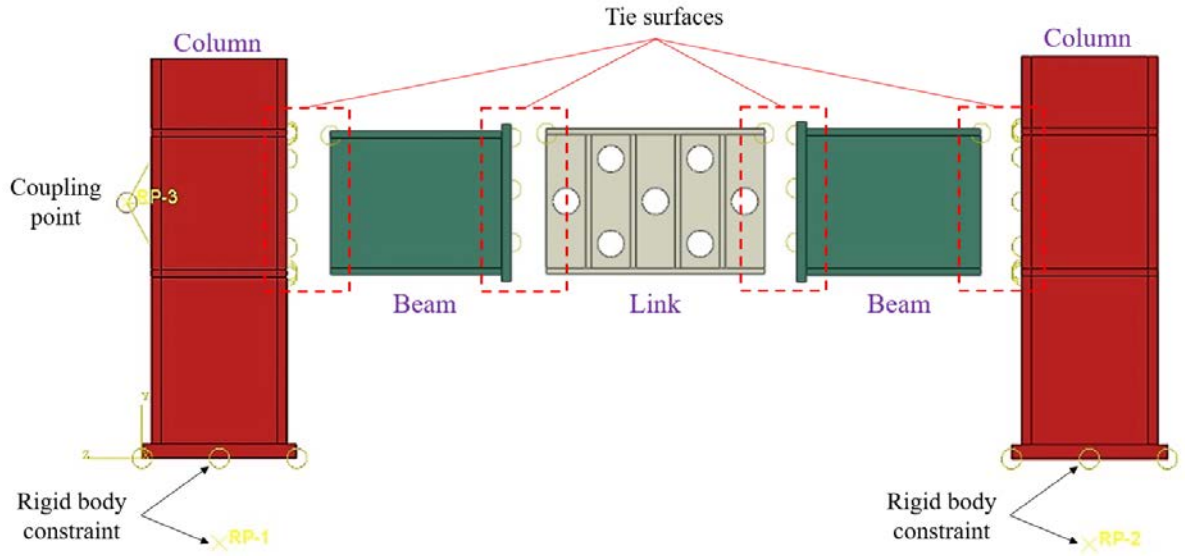

Fig. 3. Considered constraints between modeled parts

To replicate the boundary conditions of the experimental specimen, lateral constraints in the x-direction were applied at the top of the columns to prevent any out-of-plane movements (Fig. 4). Additionally, as shown in Fig. 4, "Pinned" boundary conditions were assigned to the reference points at the locations of the pinned supports. The loading protocol was applied at RP-3 along the z-direction, corresponding to the hydraulic jack's position in the experimental setup.

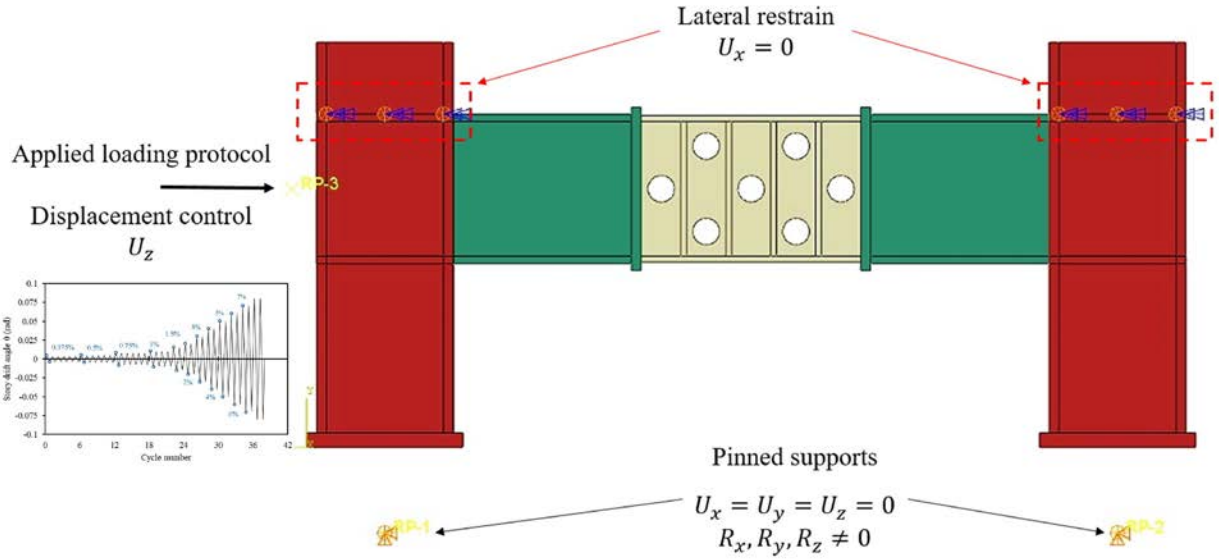

Fig. 4. Loading and boundary conditions

As illustrated in Fig. 5, a three-dimensional simulation was utilized to develop the finite element (FE) model. The various components of the model were meshed using reduced integration brick elements (C3D8R). However, in the link region, which is expected to experience significant plastic deformation and features a complex geometry with holes and stiffeners, a more precise element type (C3D10) was employed to ensure greater accuracy in the analysis.

As shown in Fig. 5, a refined mesh size of 10×10×10 mm was applied in the link region, which is expected to have high-stress concentrations, to accurately capture the localized response [37-41]. The same mesh size was utilized for the other components of the model; however, a different element type was employed in these regions (C3D8R). This ensures that while the mesh size remains consistent, a more accurate element type (C3D10) is used in the critical areas where stress concentrations are anticipated.

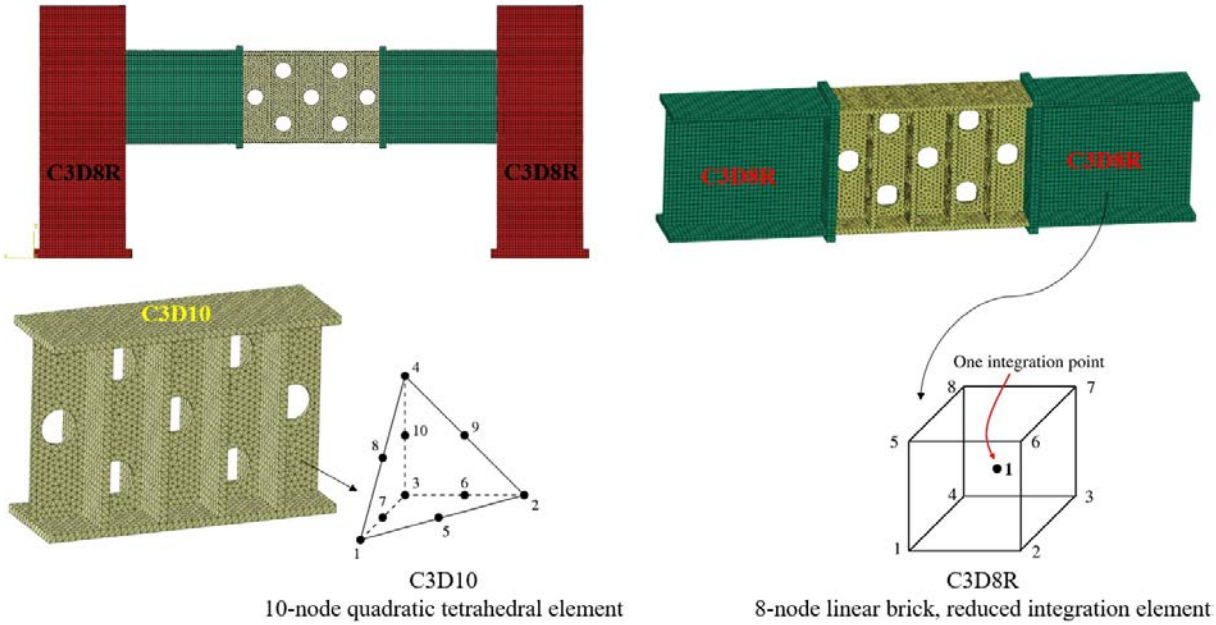

Fig. 5. Types of elements considered for meshing the FE model

The steel parts were modeled using a nonlinear material that follows the von Mises yield criterion. A combined-hardening role for steel material behavior was employed, with the measured material properties listed in Table 1. Nonlinear analysis was incorporated into the modeling process, accounting for both geometric and material nonlinearities.

Table 1. Mechanical properties of steel material [5]

Steel part	Material specification	Poisson's ratio	Elastic Modulus E/GPa	Yielding stress f_y/MPa	Ultimate stress f_u/MPa
Beam link	ST37	0.3	200	301	390
Columns Stiffeners Base plates Continuity plates	ST52	0.3	200	370	520

Fig. 6 presents a comparison of the experimental and numerical hysteresis curves. The finite element (FE) model successfully predicted both the stiffness and lateral resistance of the experimental specimen, "Pw-MRF," with a high degree of accuracy. However, a slight discrepancy was noted in the pinching behavior of the hysteresis loops, with the experimental results exhibiting a more pronounced effect than the numerical predictions, specifically in the lower right corner of the hysteretic curve. Despite this difference, the consistency of the model across all cases ensures that the comparative study between the models remains valid and unaffected.

Fig. 7 compares the deformed shapes of the experimental specimen with the analyzed model, along with the von Mises stress and equivalent plastic strain (PEEQ) distributions. The figure demonstrated a strong correlation between the experimentally observed and numerically predicted deformations of the moment-resisting frame with a shear link, observed at the end of loading at a 3% drift ratio. As shown in Fig. 7b, the model exhibits significant stress concentrations in the link region, particularly around the holes. Additionally, plastic strains were confined exclusively to the link, while the other components of the model remained elastic, showing no signs of plastic deformation (Fig. 7c). These numerical findings are consistent with the experimental observations shown in Fig. 7a, where the white paint faded only from the link region, indicating a high level of yielding.

The high level of accuracy in predicting the actual behavior underscores the effectiveness of the nonlinear simulation methodology employed in this study, particularly in capturing the local behavior of the shear link. With the model now validated, it can serve as a reliable tool for further investigation into the impact of various key parameters [42, 43].

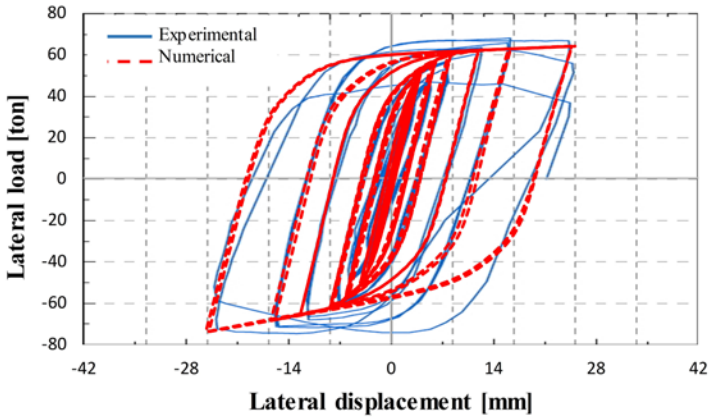

Fig. 6. Comparison of hysteretic curves between experimental and numerical studies

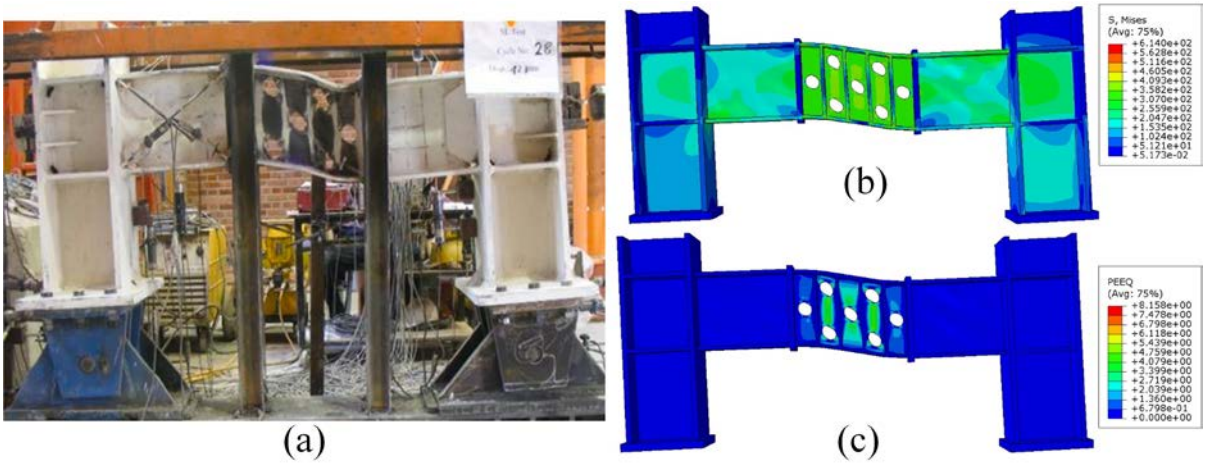

Fig. 7. Comparison of deformed shapes at 3% drift ratio: (a) experimental [5], (b) von Mises stress contour, and (c) equivalent plastic strain contour

3.2 Parametric study

Following the validation of the developed model, it was employed to investigate various parameters of the shear link and their impact on the cyclic behavior of the moment-resisting frame. While the flange geometry and web plate thickness were kept constant, as per the validated model, changes were made by removing the stiffeners and replacing the flat web plate with a corrugated one. Variations in corrugation angle, holes layout, and holes shape were explored. A uniform trapezoidal corrugation pattern was applied consistently across all models. The resulting hysteretic curves were then compared to reference specimens: a conventional moment-resisting frame studied by Mahmoudi et al. [6], and a similar frame, but incorporating a shear link at the beam midspan with a perforated and stiffened web plate, as studied by Mirghaderi et al. [5].

The goal of the proposed models was to achieve the lateral resistance capacity of a conventional moment-resisting frame using optimized shear links. It is important to note that the shear link was intentionally weakened to ensure that the demands transferred to adjacent regions did not exceed the flexural yielding capacity of the original beam. This approach ensures that only the shear link region behaves as a ductile fuse, while the other components remain elastic. For each investigated parameter, a separate group of models was developed, and the results were presented individually to facilitate comprehensive analysis.

3.2.1 Effect of corrugation angle

In this group of models, the corrugation angle was varied to examine its effect on the cyclic behavior of the moment-resisting frame. As depicted in Fig. 8, three different angles (30°, 45°, and 60°) were considered for the trapezoidal corrugated web plate, with the 30° angle being evaluated both with and without perforations. The layout angle of the holes was set at 45°, consistent with the reference specimen from Mirghaderi et al. [5]. It is important to note that the slight variation in the diameter-to-spacing (D/S) ratio between models arises from the

need to adjust the holes' placement as the corrugation angle changes. These adjustments ensured the layout angle remained constant, resulting in variations in the spacing between the holes (S).

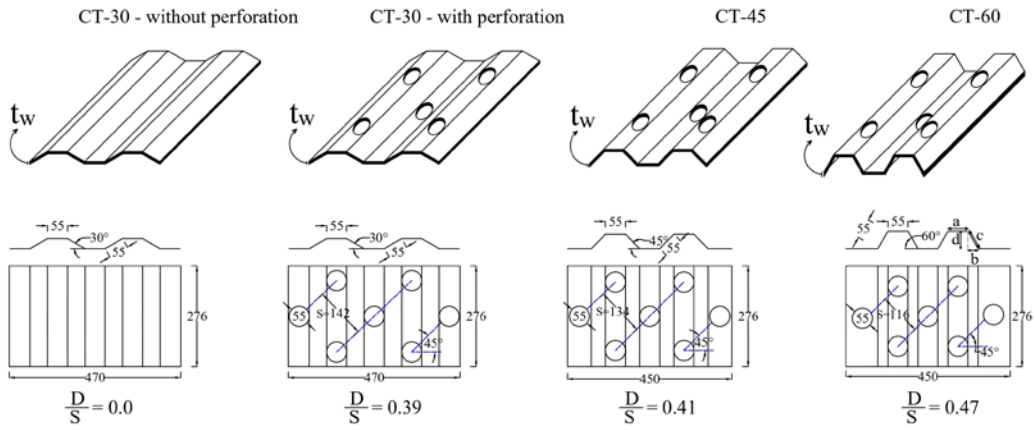

Fig. 8. Geometrical illustration of Group-1 models [mm]

Fig. 9 illustrates the hysteretic curves for the first group of models, alongside the hysteretic curve for the reference specimen "Pw-MRF". It is important to note that the curve for specimen "Pw-MRF" was included from the previous validation study. In the case of the conventional moment-resisting frame specimen conducted by Mahmoudi et al. [6], no detailed model simulation was required. Instead, the comparison was based on the maximum lateral resistance capacity of this specimen against the results from the analyzed models.

As shown in Fig. 9, all models demonstrated stable hysteretic loops without any pinching. Among the perforated specimens, the model with a 30° corrugation angle (CT-30-with perforation) exhibited the highest lateral capacity, particularly in the elastic stage, making this angle the optimal choice for the trapezoidal corrugated web plate. Conversely, when no perforations were applied to the web plate at this same angle (CT-30-without perforation), the shear link showed even higher lateral capacity. In other words, introducing perforations in the model with a 30° corrugation angle resulted in approximately a 37% reduction in the maximum lateral capacity of the frame compared to the non-perforated case. This reduction ratio closely aligns with the 39% reduction ratio $(1 - D/S)$ provided in Eq. 4.

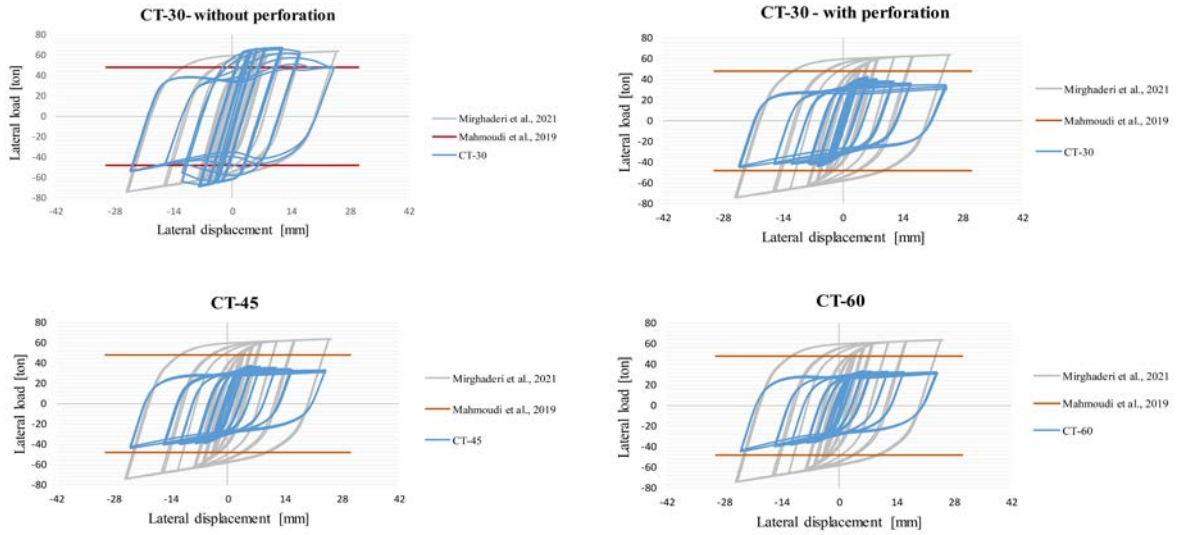

Fig. 9. Hysteretic behavior curves of Group-1 models compared to the reference specimens

For additional clarity, Fig. 10 illustrates the pushover curves of the analyzed models from this group, alongside those of the reference specimens. Notably, the model "CT-30-without perforations" outperformed the reference

specimens in terms of strength and stiffness. However, this level of strength is not required, as it may transfer excessive demands to adjacent regions, potentially causing them to contribute to the lateral capacity, which undermines the intended role of the shear link as a fuse. Despite this, all models with perforated webs in this group exhibited slightly lower lateral capacities compared to the conventional moment-resisting frame. The largest observed difference was 30%, as seen in specimen CT-60, indicating that a corrugation angle of 60° is the least favorable choice among the angles investigated.

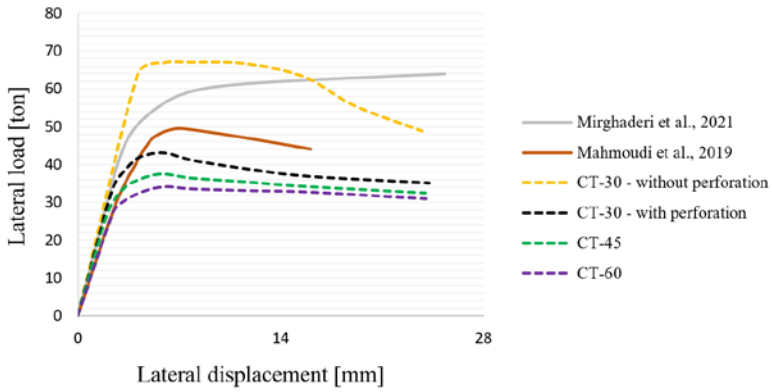

Fig. 10. Comparison of pushover curves between Group-1 models and reference specimens

In Fig. 11, the considered models are presented alongside their deformed shapes, as well as the von Mises stress and equivalent plastic strain contours for this group. Clearly, the use of a shear link at the beam midspan led to stress concentration in this region, effectively functioning as a ductile fuse. For the CT-30 model without perforations, the higher demands transferred from the fuse to the adjacent regions resulted in these areas contributing to the lateral-resisting capacity. Notably, the webs of the beams adjacent to the link in this model showed slight deformation and buckling, highlighting the significant lateral capacity of this model compared to those with perforated links, which resulted from the combined contribution of the fuse and the adjacent beams, suggesting it may be prudent to exclude this model from comparative analyses in future investigations.

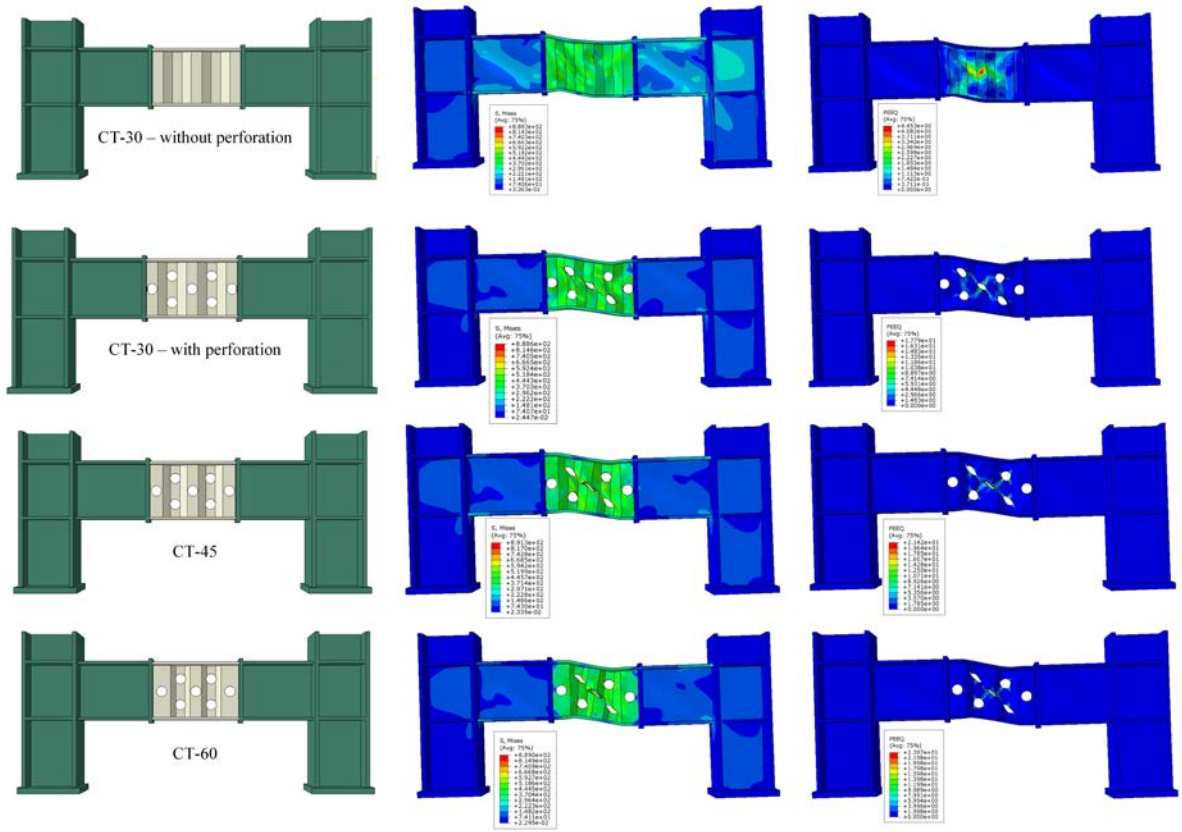

Fig. 11. Deformed shapes, von Mises stress contours, and PEEQ contours for Group-1 models

In contrast, the models with perforated links demonstrated yielding in the link region (fuse), while the other components of the frame remained elastic. Furthermore, among the perforated models, the link with a corrugation angle of 60° (CT-60 model) exhibited the highest maximum equivalent plastic strains (PEEQ = 2.397) compared to the models with 30° and 45° angles, indicating a more critical condition in this scenario.

The hysteresis curves shown in Fig. 9 can be utilized to calculate the plastic energy dissipated across the analyzed models. The term "plastic dissipation energy" refers to the area enclosed within each hysteresis loop, representing the energy lost due to irreversible plastic deformations [30]. Fig. 12 illustrates the plastic dissipation energy for models with perforated and corrugated webs in comparison to the validated reference specimen. As depicted in the figure, none of the proposed models achieved the level of dissipated energy observed in the reference specimen. Among the analyzed models, the one with a 30° corrugation angle exhibited the highest dissipation energy. However, the differences in the amount of dissipated energy among the proposed models were not significant, where the dissipated energy remained relatively constant for all models, including the reference model, during the initial stages of loading.

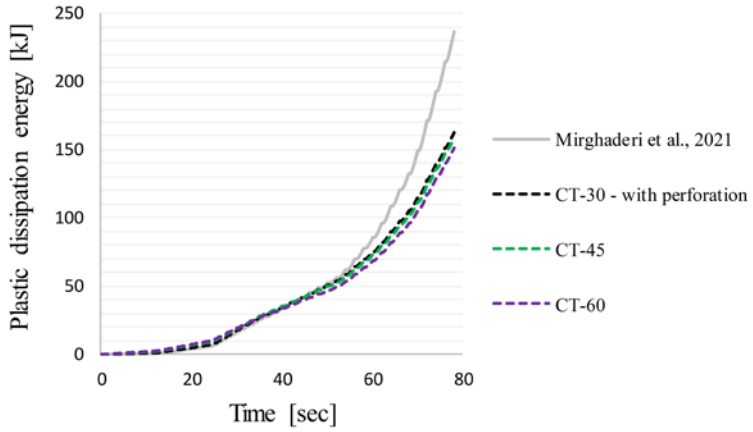

Fig. 12. Comparison of plastic dissipation energy between Group-1 models

The models in this group indicated that the optimum angle for the trapezoidal corrugated web plate of the link was 30°, as it exhibited superior capacity and greater energy dissipation compared to models with links featuring 45° and 60° corrugated web plates. Furthermore, the shear link should be designed to be weaker than the adjacent beams to ensure that its function as a ductile fuse is preserved without relying on contributions from other regions of the system. This design approach facilitates the expected performance of the proposed system.

3.2.2 Effect of holes' layout

In this group of models, the layout of the holes was identified as a key parameter to be studied. This parameter is influenced by the hole diameter (D) and the spacing between the holes (S). As shown in Fig. 13, the corrugation angle was fixed at 30° across all models. Three hole diameters were evaluated: 38 mm, 41 mm, and 51 mm. For each diameter, different layouts were applied, with the layout angle remaining constant at 45°. Notably, for the 51 mm diameter, two distinct layouts were investigated to specifically assess the impact of hole arrangement for a fixed diameter.

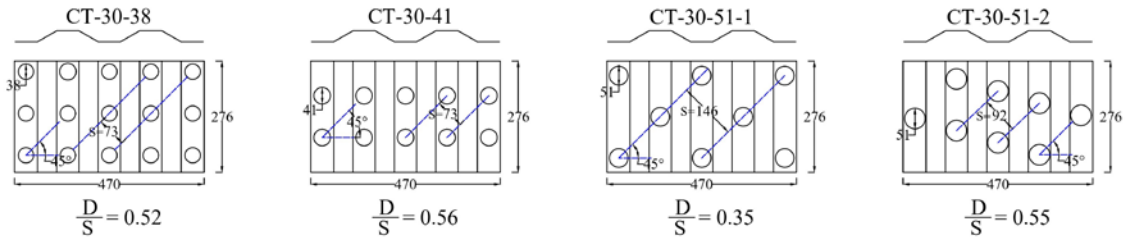

Fig. 13. Geometrical illustration of Group-2 models [mm]

Fig. 14 illustrates the hysteresis curves of the models of this group subjected to cyclic loading, compared to reference models. Notably, even though the material and geometrical properties of the shear links remained

constant compared to the previous group of models, using smaller hole diameters with a more uniform distribution led to an improvement in the maximum lateral capacity of the moment frames. As a result, nearly all models achieved the lateral capacity of the conventional moment-resisting frame. Although the model CT-30-51-1 with a 51 mm hole diameter matched the lateral capacity of the reference model, the model CT-30-51-2, despite having the same hole diameter, failed to reach the same capacity. This highlights the critical importance of considering a uniform hole layout, even when the layout angle and hole diameter remain constant. Furthermore, in model CT-30-38, the use of a smaller hole diameter with a more distributed arrangement within the link web plate area resulted in improved cyclic performance. The hysteresis loops for this model displayed greater stability without compromising ultimate lateral capacity. Although none of the proposed models could match the lateral capacity of the reference specimen from Mirghaderi et al. [5], achieving the lateral capacity of the conventional moment-resisting frame [1] with similar characteristics is sufficient for this study. It should be noted that Mirghaderi et al.'s model incorporated a stronger link due to the inclusion of many stiffeners between the holes within the web plate.

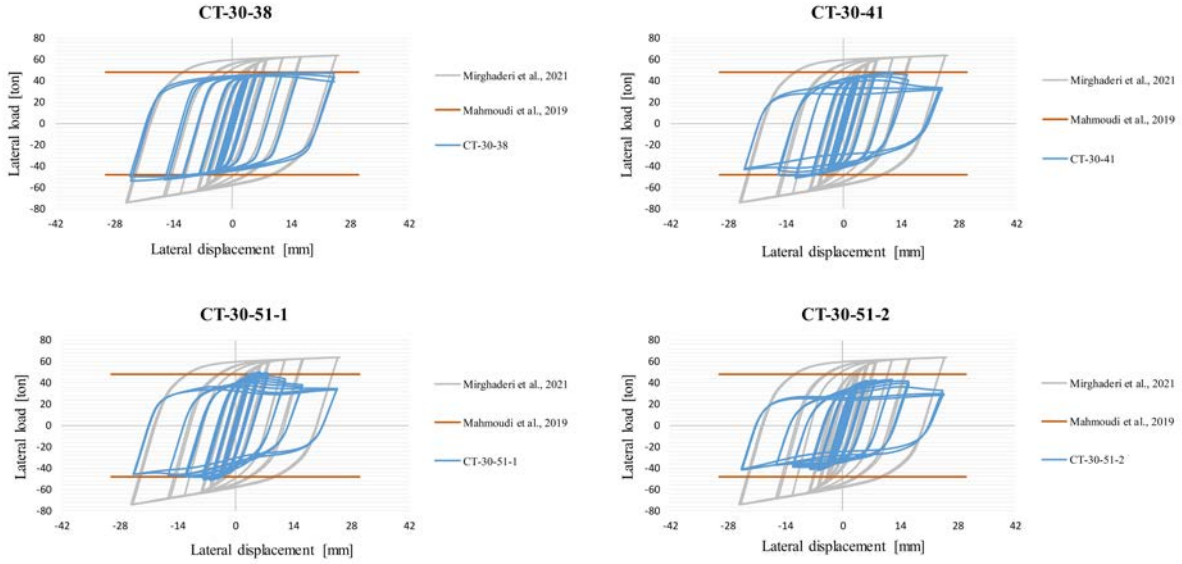

Fig. 14. Hysteretic behavior curves of Group-2 models compared to the reference specimens

In Fig. 15, the pushover curves of the analyzed models are presented, along with those of the reference specimens. It is important to note that the CT-30 model with perforations from the previous group was included for comparison. As illustrated in the figure, the models with shear links exhibited higher stiffness than the reference specimen of a conventional moment-resisting frame with similar characteristics. Among all models in this group, model CT-30-38 demonstrated stable behavior, maintaining its plastic stiffness hardening even at large drift ratios. While model CT-30-51-1 achieved the highest maximum lateral resisting capacity, it experienced a significant drop in strength after reaching its peak at an early stage of loading.

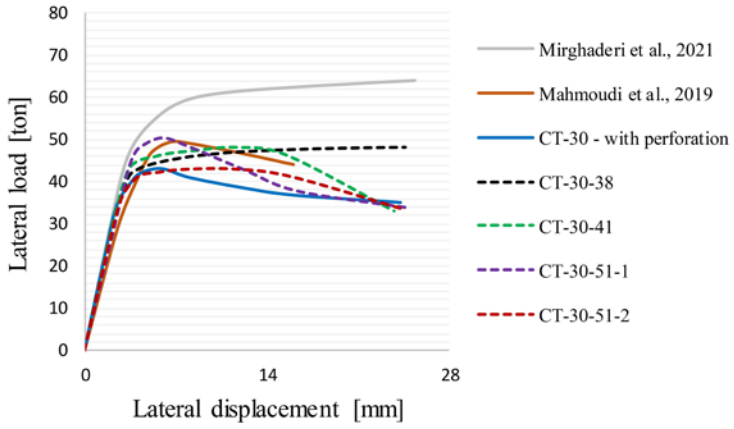

Fig. 15. Comparison of pushover curves between Group-2 models and reference specimens

Interestingly, despite the hole diameter reduction of only about 7% (from 55 mm to 51 mm) between the CT-30-perforated model and CT-30-51-1, where a D/S ratio reduction of approximately 10%, the ultimate lateral capacity improved by around 17% between the two models. However, as seen in model CT-30-51-2, despite using a smaller hole diameter compared to the CT-30 model with perforations, the ultimate lateral capacity did not improve. This highlights the critical importance of employing a more uniform distribution for holes and a lower D/S ratio for a better performance of the shear link.

Fig. 16 presents the FE models for this group, showing their deformed shapes, von Mises stress distributions, and equivalent plastic strain (PEEQ) contours. Across all models, yielding was concentrated in the link region, acting as a ductile fuse in the load-transferring chain, while areas outside this region remained elastic during analysis.

Regarding the equivalent plastic strain contour, it is evident that using a perforated web plate with smaller, more distributed holes increased the web plate's contribution to resisting applied loads, resulting in stable hysteresis behavior and remarkable lateral resistance, as shown in Figs. 14 and 15. Specifically, reducing the D/S ratio improved performance by lowering plastic strain concentrations. This was clear in model CT-30-38, where the maximum PEEQ value was about 10.77, showing a maximum difference of about 25% compared to the CT-30-51-2 model with a maximum PEEQ value of 13.48.

Despite both CT-30-51 models having the same hole diameter, the plastic strain varied based on the layout of the holes. The uniform distribution in CT-30-51-1 led to a more distributed plastic strain, avoiding high-stress concentrations. In contrast, model CT-30-51-2 exhibited a 4.3% increase in the PEEQ index, highlighting that a more uniform distribution with a smaller hole diameter (lower D/S ratio) is preferred when designing such shear links for moment frames.

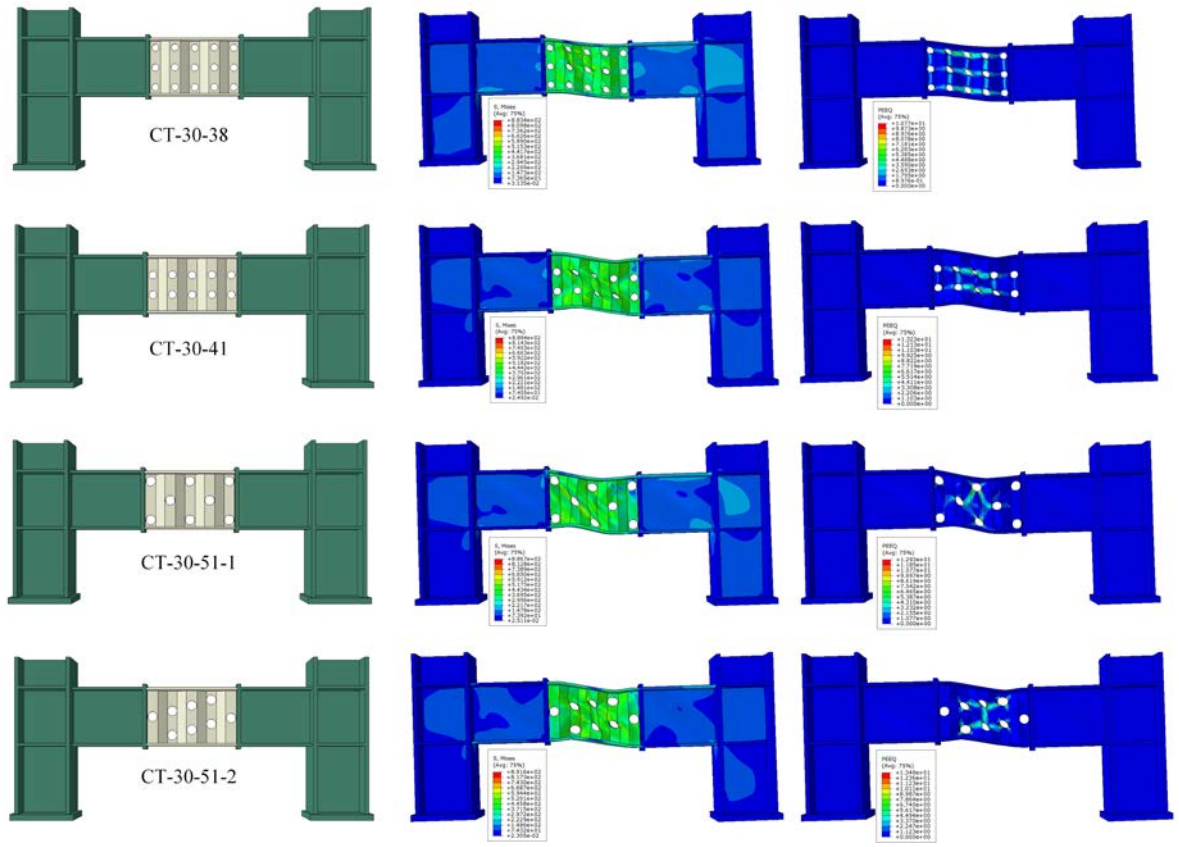

Fig. 16. Deformed shapes, von Mises stress contours, and PEEQ contours for Group-2 models

Fig. 17 illustrates the plastic dissipation energy for this group of models, compared with both the reference specimen from Mirghaderi et al. [5] and the CT-30 model with perforation. Notably, reducing the D/S ratio in this group of models led to an increase in energy dissipation; the lower the D/S ratio, the higher the dissipation energy observed.

Although the shear link in the reference specimen exhibited a higher lateral capacity due to the use of stiffeners, the CT-30-38 model, which had a lower D/S ratio without stiffeners, achieved nearly the same dissipation energy. The difference between CT-30-38 and the reference specimen was approximately 16% at the final loading stage. However, all models showed similar levels of plastic dissipation energy during the initial stage of loading.

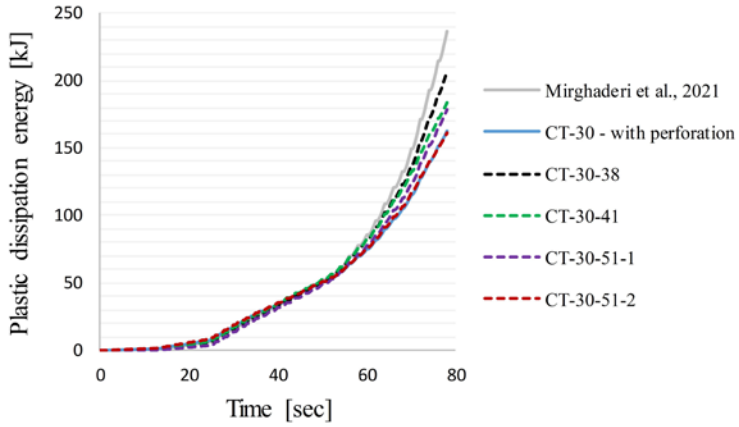

Fig. 17. Comparison of plastic dissipation energy between Group-2 models

The findings from this group of models emphasize that for the proposed shear links, it is essential to adopt a uniform layout for the holes with smaller diameters, reducing the D/S ratio while keeping the layout angle at 45°. This approach significantly improved the cyclic performance of the moment frame, providing more stable hysteresis loops, better plastic strain and stress distribution, and an enhanced ultimate lateral resistance capacity.

3.2.3 Effect of holes' shape

As shown in Fig. 18, the models in this group are similar to those in Group-2, with the primary difference being the shape of the holes. In this group, the circular holes seen in Fig. 13 were replaced with elliptical holes of the same area. The goal was to explore potential enhancements in the overall behavior by using elliptical holes, which are better suited to the geometry of the corrugated web plate. For consistency and comparison purposes, the layout of the Group-2 models was kept unchanged.

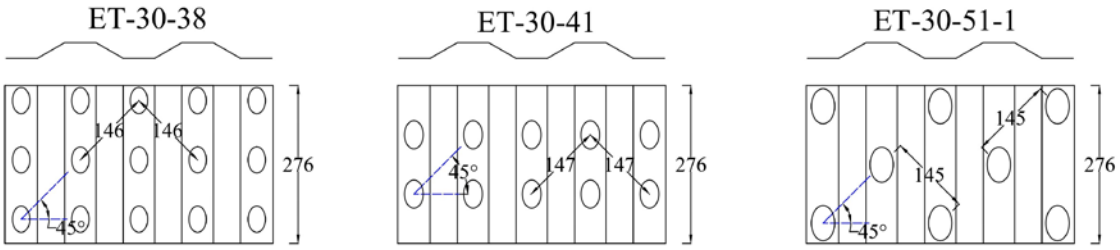

Fig. 18. Geometrical illustration of Group-3 models [mm]

The hysteretic curves presented in Fig. 19 demonstrate that all models were able to achieve the ultimate lateral resistance capacity of the conventional moment-resisting frame with similar characteristics. However, consistent with the conclusions drawn from the Group-2 models, reducing the diameter-to-spacing (D/S) ratio led to more stable hysteresis loops, avoiding softening in the curves in the plastic stage. This behavior is particularly evident in model ET-30-38, which had the lowest D/S ratio.

In comparison to the models in Group-2, the overall behavior showed no significant changes, as evident from the pushover curves in Fig. 20. This indicates that the shape of the holes had no substantial impact on the stiffness, lateral capacity, or hysteretic behavior of the proposed models.

The models in this group, along with their deformed shapes, stress distributions, and plastic strain contours, are illustrated in Fig. 21. It is evident that the shear link acted as the ductile fuse, with yielding and plastic strains concentrated solely in the link region for all models. Notably, the PEEQ values decreased when the hole shape was altered from circular to elliptical. The reductions were approximately 17%, 8%, and 6% for models ET-30-38, ET-30-41, and ET-30-51-1, respectively, when compared to models CT-30-38, CT-30-41, and CT-30-51-1. This suggests that the shape of the holes significantly influences the enhancement of plastic deformations within the link region, especially for lower models with a lower D/S ratio, thereby reducing the concentration of plastic strains and PEEQ values accordingly.

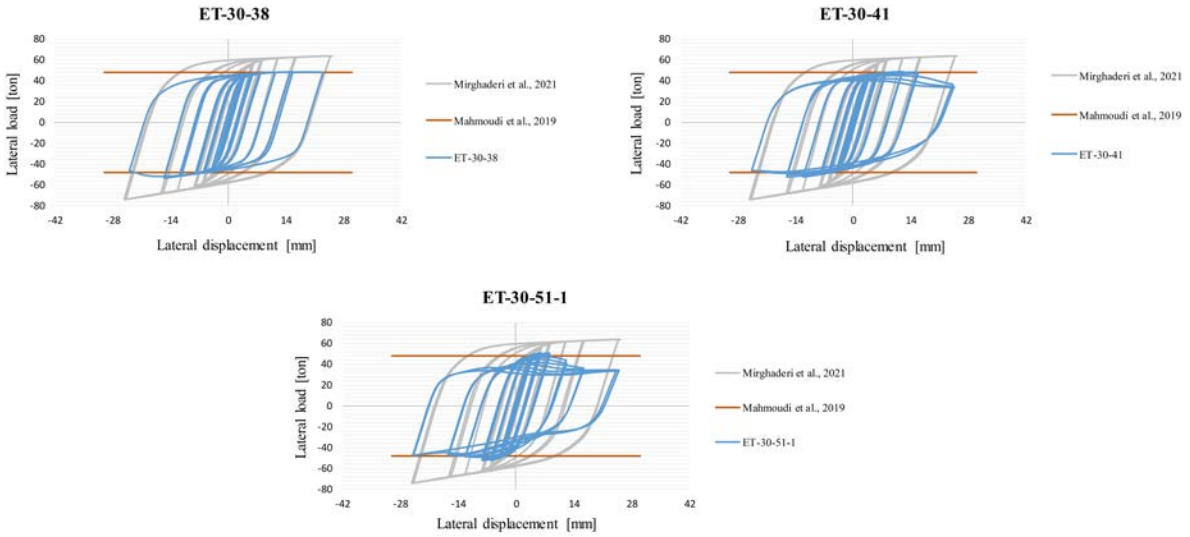

Fig. 19. Hysteretic behavior curves of Group-3 models compared to the reference specimens

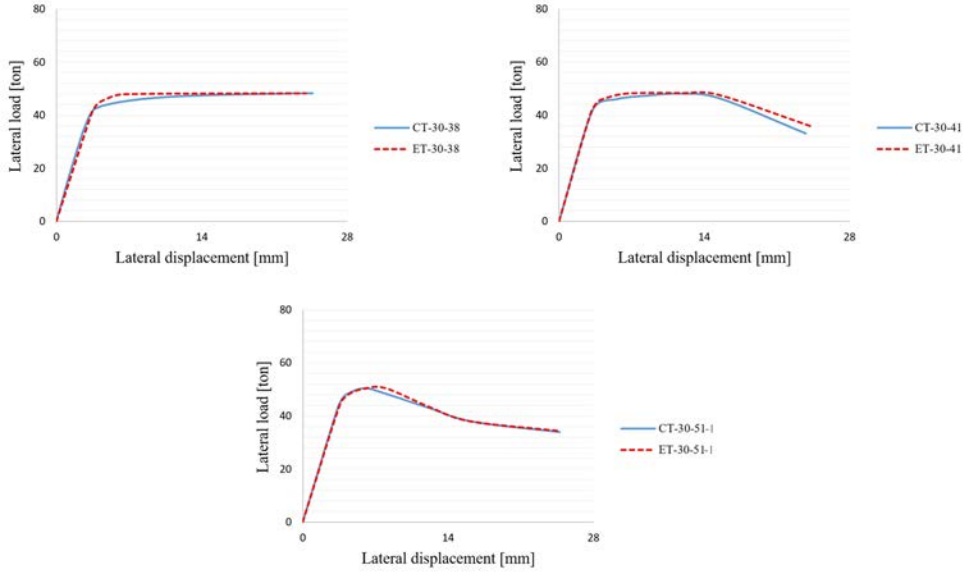

Fig. 20. Comparison of pushover curves between Group-2 and Group-3 models

However, since the hysteretic loops of this group were identical to those of Group-2 (Figs. 19 and 20), the change in hole shape from circular to elliptical did not affect the plastic dissipation energy, as illustrated in Fig. 22.

The findings from this group highlighted that the shape of the holes significantly contributed to reducing the concentration of plastic strains in the link region by creating a more evenly distributed yielding area within the web plate. However, it did not affect the overall behavior of the moment frames with the proposed shear links.

3.3 Comparison study

In this subsection, a comparison of the most critical findings was made among all analyzed models and the reference specimens. Fig. 23 illustrates the maximum lateral capacity achieved by each analyzed model in relation to the reference specimens. As depicted, the lateral capacity of Mirghaderi et al.'s specimen was not achieved by any of the analyzed models. This discrepancy can be attributed to the shear link used in their specimen, which was reinforced with numerous stiffeners, resulting in a higher lateral capacity than that of the conventional moment-resisting frame with similar characteristics. Achieving this higher capacity was not a goal of the current study.

In contrast, all models with a corrugation angle of 30° demonstrated a lateral capacity comparable to that of the reference specimen of the conventional moment-resisting frame with equivalent characteristics. However, the models with corrugation angles of 45° and 60° exhibited lower lateral capacities compared to the other models.

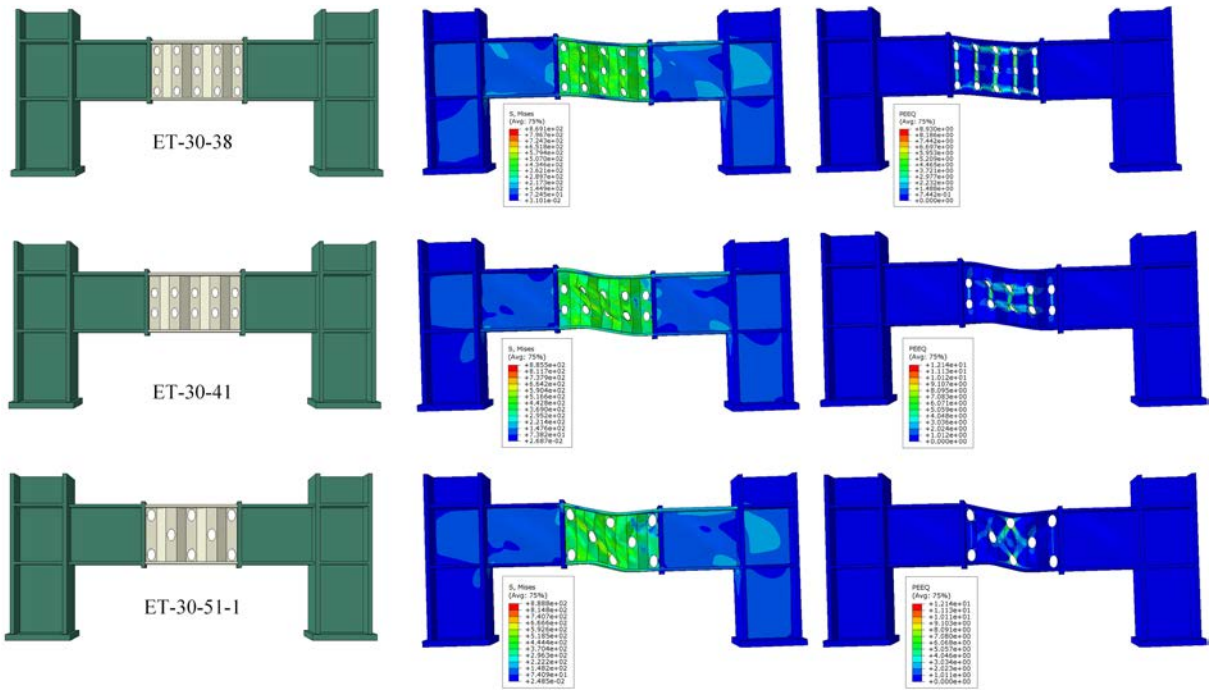

Fig. 21. Deformed shapes, von Mises stress contours, and PEEQ contours for Group-3 models

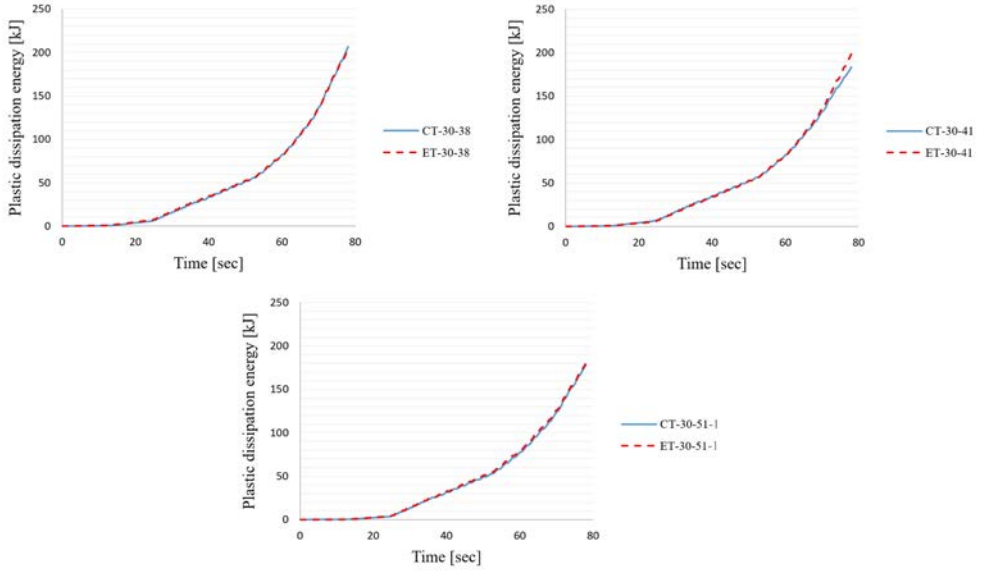

Fig. 22. Comparison of plastic dissipation energy between Group-2 and Group-3 models

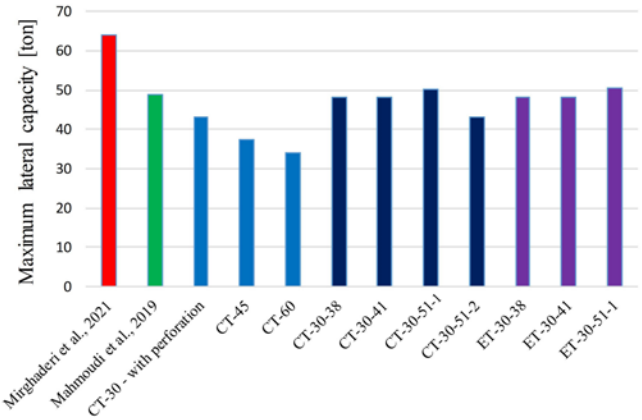

Fig. 23. Comparison of maximum lateral capacity across analyzed models

Fig. 24 presents the PEEQ values for the analyzed models. It is evident that the PEEQ values decrease as the D/S ratio is reduced and when elliptical-shaped holes are implemented. However, the presence of multiple stiffeners in Mirghaderi et al.'s specimen resulted in lower PEEQ values, as the link region was significantly stiffened, making it stronger than the models developed without stiffeners. It is important to note that the analysis did not account for the effects of stress and strain concentrations resulting from welding, which could potentially elevate the PEEQ values under real-world conditions.

Fig. 25 depicts the maximum plastic dissipation energy for each analyzed model for comparison. Clearly, models featuring a more uniform distribution of smaller-diameter holes (resulting in a lower D/S ratio) exhibited a greater amount of dissipated energy. Additionally, a slight improvement in energy dissipation was observed when circular holes were alternated with elliptical holes of the same perforation area. The corrugation angle did not significantly influence the maximum dissipation energy among models. Notably, the reference specimen with the strengthened web demonstrated the highest level of plastic dissipation energy, with a maximum difference of approximately 16% compared to the proposed models.

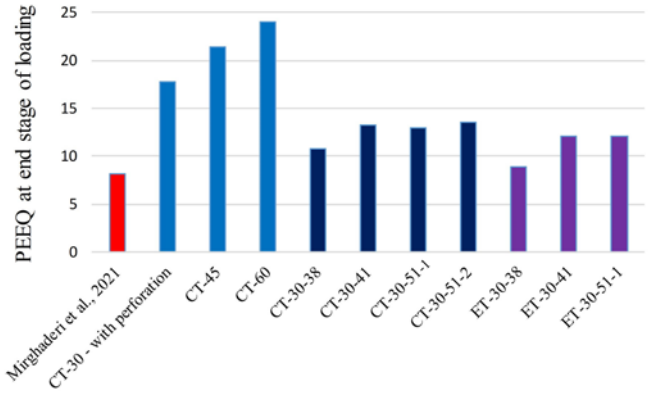

Fig. 24. Comparison of equivalent plastic strain index (PEEQ) across analyzed models

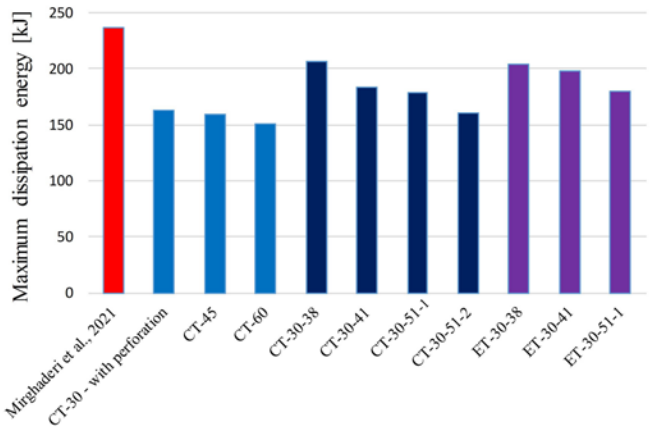

Fig. 25. Comparison of maximum dissipation energy across analyzed models

4. Summary and conclusions

This study presented a comprehensive numerical investigation into the cyclic performance of moment-resisting frames featuring corrugated and perforated shear links located at the beam midspan. The finite element method was employed, incorporating geometrical and material nonlinear analysis to accurately capture the complex response of shear links under cyclic loading conditions. Key parameters influencing the performance of the shear links were meticulously considered, including the corrugation angle, the geometric shape of the holes, and the layout of the holes. The findings of this study are summarized as follows:

1) The proposed shear link represented a viable alternative design solution for moment-resisting frames with short spans, where adherence to the length-to-depth ratio limitations is unavoidable. The proposed structural system demonstrated satisfactory cyclic performance, characterized by significant energy dissipation, high lateral-resistance capacity, and high ductility.

2) For all the models, yielding was concentrated in the shear link region rather than resulting in the formation of plastic hinges at the ends of the flexural beam. As a result, the other components of the moment frame remained within the elastic stage.

3) For all models, the proposed moment frame system exhibited greater ductility compared to its conventional moment-resisting frame counterpart with similar characteristics.

4) Employing a suitable layout for the holes with a lower D/S (diameter-to-spacing) ratio reduced plastic strains, leading to more stable hysteresis loops without a significant reduction in lateral capacity, even at large drift ratios. However, the D/S ratio had a trivial effect on the lateral resisting capacity of the moment frame when the corrugation angle is constant (30 degrees in this study).

5) Enhancing the layout of the holes by utilizing smaller diameters and a more uniform distribution resulted in achieving lateral capacity comparable to that of conventional moment-resisting frames with identical characteristics.

6) Using shear links with a corrugation angle of 30° yielded a higher lateral capacity compared to those with corrugation angles of 45° and 60°. However, the plastic dissipation energy was relatively insensitive to the corrugation angle, as the amount of energy dissipated remained nearly constant across all models.

7) The shape of the holes, whether circular or elliptical with equivalent areas, did not influence the lateral resistance capacity or the amount of energy dissipation of the proposed moment frames. However, using elliptical holes significantly contributed to reducing the concentration of plastic strains in the link region by creating a more evenly distributed yielding area within the web plate.

8) The deformability and energy dissipation improved with a more uniform distribution layout and smaller hole diameters. In other words, reducing the D/S ratio by adjusting the hole diameter and layout (while maintaining a perforation angle of 45°) significantly enhanced the lateral capacity, energy dissipation, and the shape of the hysteresis loops of the moment frame. This improvement occurred because a larger region of the shear link yielded, thereby contributing to the resistance against the applied load.

9) All models demonstrated the ability to achieve the lateral capacity of conventional moment-resisting frames with identical characteristics. Furthermore, some models reached levels of energy dissipation comparable to those observed in shear links featuring flat perforated webs with stiffeners. This is noteworthy, as the steel material used in the stiffened models is significantly greater than that employed in the proposed models, which do not incorporate stiffeners or welds.

In summary, this study primarily investigated the cyclic behavior and structural response of the proposed shear link, revealing several intrinsic advantages over conventional shear links with flat webs and internal stiffeners, particularly in terms of fatigue resistance and long-term durability. The strategic elimination of internal stiffeners significantly reduces stress concentrations and potential crack initiation sites commonly associated with welded connections. Coupled with a marked reduction in welding, this approach not only minimizes residual stresses and heat-affected zones, both detrimental to fatigue life, but also streamlines the fabrication process, enhancing overall efficiency. Complementing these benefits, the adoption of a bolted connection system facilitates easier inspection, maintenance, and replacement, thereby extending the service life and adaptability of the shear link.

Although this research primarily relied on numerical simulations to analyze stress distribution, plastic strain evolution, and overall stability under cyclic loading, the results provide valuable insights and establish a robust groundwork for future experimental validation. To fully evaluate the performance and durability of the proposed system under practical service conditions, further research incorporating full-scale fatigue testing and long-term monitoring is strongly recommended.

5. References

[1] Nikoukalam M, Dolatshahi KM. Development of structural shear fuse in moment resisting frames. Journal of Constructional Steel Research. 2015;114:349-361. https://doi.org/10.1016/j.jcsr.2015.08.008

[2] AISC-358. Prequalified connections for special and intermediate steel moment frames for seismic applications: American Institute of Steel Construction. USA. 2022.

[3] AISC-341. Seismic provisions for structural steel buildings: American Institute of Steel Construction. USA. 2022.

[4] Taranath BS. Structural analysis and design of tall buildings: Steel and composite construction: CRC press; 2016.

[5] Mirghaderi SR, Mahmoudi B, Gharavi A, Dolatshahi KM, Epackachi S. Experimental investigation of moment resisting frames with perforated shear link. Structures. 2021;32:516-531. https://doi.org/10.1016/j.istruc.2021.03.060

[6] Mahmoudi F, Dolatshahi KM, Mahsuli M, Nikoukalam MT, Shahmohammadi A. Experimental study of steel moment resisting frames with shear link. Journal of Constructional Steel Research. 2019;154:197-208. https://doi.org/10.1016/j.jcsr.2018.11.027

[7] Dolatshahi KM, Gharavi A, Mirghaderi SR. Experimental investigation of slitted web steel moment resisting frame. Journal of Constructional Steel Research. 2018;145:438-448. https://doi.org/10.1016/j.jcsr.2018.03.004
[8] Kalehbasti PR, Dolatshahi KM. Two novel shear fuses in moment resisting frames. Journal of Constructional Steel Research. 2018;144:198-210. https://doi.org/10.1016/j.jcsr.2018.01.026
[9] Hoseinzadeh Asl M, Jahanian M. Behaviour of Steel Deep Beams in Moment Frames with Web Opening Subjected to Lateral Loading. International Journal of Steel Structures. 2020;20:1482-1497. https://doi.org/10.1007/s13296-020-00381-x
[10] Mansouri A, Sharif MM. Development of a corrugated web shear link for steel moment-resisting frames. Journal of Constructional Steel Research. 2022;193:107281. https://doi.org/10.1016/j.jcsr.2022.107281
[11] Abbas HH, Sause R, Driver RG. Behavior of corrugated web I-girders under in-plane loads. Journal of Engineering Mechanics. 2006;132(8):806-814. https://doi.org/10.1061/(ASCE)0733-9399(2006)132:8(806)
[12] Elgaaly M, Hamilton RW, Seshadri A. Shear strength of beams with corrugated webs. Journal of Structural Engineering. 1996;122(4):390-398. https://doi.org/10.1061/(ASCE)0733-9445(1996)122:4(390)
[13] Driver RG, Abbas HH, Sause R. Shear behavior of corrugated web bridge girders. Journal of structural engineering. 2006;132(2):195-203. https://doi.org/10.1061/(ASCE)0733-9445(2006)132:2(195)
[14] Eldib M-H. Shear buckling strength and design of curved corrugated steel webs for bridges. Journal of Constructional Steel Research. 2009;65(12):2129-2139. https://doi.org/10.1016/j.jcsr.2009.07.002
[15] Bahrebar M, Lim JB, Clifton GC, Zirakian T, Shahmohammadi A, Hajsadeghi M. Perforated steel plate shear walls with curved corrugated webs under cyclic loading. Structures. 2020;24:600-609. https://doi.org/10.1016/j.istruc.2020.01.047
[16] Emami F, Mofid M. On the hysteretic behavior of trapezoidally corrugated steel shear walls. The Structural Design of Tall and Special Buildings. 2012;23(2):94-104. https://doi.org/10.1002/tal.1025
[17] Emami F, Mofid M, Vafai A. Experimental study on cyclic behavior of trapezoidally corrugated steel shear walls. Engineering Structures. 2013;48:750-762. https://doi.org/10.1016/j.engstruct.2012.11.028
[18] Farzampour A, Mansouri I, Lee C-H, Sim H-B, Hu JW. Analysis and design recommendations for corrugated steel plate shear walls with a reduced beam section. Thin-walled structures. 2018;132:658-666. https://doi.org/10.1016/j.tws.2018.09.026
[19] Hosseinzadeh L, Emami F, Mofid M. Experimental investigation on the behavior of corrugated steel shear wall subjected to the different angle of trapezoidal plate. The Structural Design of Tall and Special Buildings. 2017;26(17):e1390. https://doi.org/10.1002/tal.1390
[20] Hosseinzadeh L, Mofid M, Aziminejad A, Emami F. Elastic interactive buckling strength of corrugated steel shear wall under pure shear force. The Structural Design of Tall and Special Buildings. 2017;26(8):e1357. https://doi.org/10.1002/tal.1357
[21] Qiu J, Zhao Q, Yu C, Li Z. Experimental studies on cyclic behavior of corrugated steel plate shear walls. Journal of Structural Engineering. 2018;144(11):04018200. https://doi.org/10.1061/(ASCE)ST.1943-541X.0002165
[22] Zhao Q, Sun J, Li Y, Li Z. Cyclic analyses of corrugated steel plate shear walls. The Structural Design of Tall and Special Buildings. 2017;26(16):e1351. https://doi.org/10.1002/tal.1351
[23] Shahmohammadi A, Mirghaderi R, Hajsadeghi M, Khanmohammadi M. Application of corrugated plates as the web of steel coupling beams. Journal of Constructional Steel Research. 2013;85:178-190. https://doi.org/10.1016/j.jcsr.2013.02.009
[24] Zirakian T, Hajsadeghi M, Lim JB, Bahrebar M. Structural performance of corrugated web steel coupling beams. Proceedings of the Institution of Civil Engineers-Structures and Buildings. 2016;169(10):756-764. https://doi.org/10.1680/jstbu.15.00026
[25] Hosseinpour E, Baharom S, Yadollahi Y. Evaluation of steel shear walls behavior with sinusoidal and trapezoidal corrugated plates. Advances in Civil Engineering. 2015;2015(1):715163. https://doi.org/10.1155/2015/715163
[26] AISC-360. Specification for structural steel buildings: American Institute of Steel Construction. USA. 2016.
[27] Bruneau M, Uang CM, Saelli R. Ductile Design of Steel Structures: New York: McGraw-Hill. 2011.
[28] JSCE. Design Manual for PC bridges with corrugated steel webs. Research Commitee for Hybrid Structure with Corrugated Steel Webs: Japan Society of Civil Engieering. Japan. 1998.
[29] Sayed-Ahmed EY. Behaviour of steel and (or) composite girders with corrugated steel webs. Canadian Journal of Civil Engineering. 2001;28(4):656-672. https://doi.org/10.1139/l01-027
[30] Abaqus. Dassault systemes simulia corporation. Providence, Rhode Island, USA. 2019.
[31] Ali M. Welded anchor rods for column base connections: figshare. Thesis. 2025. https://doi.org/10.6084/m9.figshare.28795181.v1

[32] Ali M, Mirghaderi SR, Ghiami Azad AR. Investigating the effectiveness of concentric welded anchor rods in column base plate connections: A numerical and experimental study. Structures. 2024;65:106698. https://doi.org/10.1016/j.istruc.2024.106698
[33] Ali M, Mirghaderi SR, Ghiami Azad AR. Ultimate tensile behavior of all-round fillet welds in anchor-rod to base-plate connections. Structures. 2024;70:107840. https://doi.org/10.1016/j.istruc.2024.107840
[34] Ali M, Mirghaderi SR, Ghiami Azad AR, Karami I. Special all-round fillet weld for anchor rods of base-plate T-stub connections. The Structural Design of Tall and Special Buildings. 2024;33(3):e2072. https://doi.org/10.1002/tal.2072
[35] Tajik N, Marmarchinia S, Mahmoudian A, Asghari A, Mirghaderi SR. The effect of multi-pass welding on residual stresses in fillet welded built-up steel box sections. Asian Journal of Civil Engineering. 2024;1-20. https://doi.org/10.1007/s42107-024-01218-2
[36] Marmarchinia S, Ghiami Azad AR, Mirghaderi SR, Karney B, Ali M. A novel modular system for pipe racks using friction-slip connections. Journal of Constructional Steel Research. 2025;226:109286. https://doi.org/10.1016/j.jcsr.2024.109286
[37] Ali M, Zahrai SM, Mirghaderi SR. Seismic performance of rocking braced frames with double base plate connections. Structures. 2024;61:106086. https://doi.org/10.1016/j.istruc.2024.106086
[38] Alizehi E, Ghassemieh M, Mirghaderi SR, Ali MA. Development of Near-Field Earthquake Loading Protocols for the Steel Moment Connections in Iran. Journal of Earthquake and Tsunami. 2023;17(02):2350005. https://doi.org/10.1142/S1793431123500057
[39] Al-Sharmootee M, Lavassani SHH, Hosseini MH, Ali M. The cyclic performance of column base plate connections using different types of stiffeners. Canadian Journal of Civil Engineering. 2023;54(4):449-460. https://doi.org/10.1139/cjce-2023-0156
[40] Ali M, Mirghaderi SR, Ghiami Azad AR. Innovative column base connections using welded anchor rods. Steel Construction. 2025. https://doi.org/10.1002/stco.202400039
[41] Zohdi A, Matinpour MH, Rafati Bonab R, Kiumarsi Oskuei F. Seismic performance of the enlarged beam section connection. Steel Construction. 2024;17(1):29-43. https://doi.org/10.1002/stco.202200032
[42] Bypour M, Mahmoudian A, Tajik N, Taleshi MM, Mirghaderi SR, Yekrangnia M. Shear capacity assessment of perforated steel plate shear wall based on the combination of verified finite element analysis, machine learning, and gene expression programming. Asian Journal of Civil Engineering. 2024;25:5317-5333. https://doi.org/10.1007/s42107-024-01115-8
[43] Tajik N, Mirghaderi SR, Asghari A, Hamidia M. Experimental and numerical study on weld strengths of built-up steel box columns. Journal of Constructional Steel Research. 2024;213:108362. https://doi.org/10.1016/j.jcsr.2023.108362